Optics Letters

Multimode photon-exciton coupling in an organic-dye-attached photonic quasicrystal

Kun Zhang,[1] Yue Xu,[1] Tian-Yong Chen,[1] Hao Jing,[1] Wen-Bo Shi,[1] Bo Xiong,[1] Ru-Wen Peng,[1,2] and Mu Wang[1,3]

[1]National Laboratory of Solid State Microstructures, School of Physics, and Collaborative Innovation Center of Advanced Microstructures, Nanjing University, Nanjing 210093, China
[2]e-mail: rwpeng@nju.edu.cn
[3]e-mail: muwang@nju.edu.cn

Received 10 October 2016; accepted 5 November 2016; posted 15 November 2016 (Doc. ID 278421); published 12 December 2016

In this Letter, we present hybrid strong coupling between multiple photonic modes and excitons in an organic-dye-attached photonic quasicrystal. The excitons effectively interact with the photonic modes offered by the photonic quasicrystal, and multiple hybrid polariton bands are demonstrated in both experiments and calculations. Furthermore, by retrieving the measured dispersion map, we get the mixing fractions of photonic modes and excitons, and show that the polariton bands inherit not only the energy dispersion features, but also the damping behaviors from both the photonic modes and the excitons. Our investigation may inspire related studies on multimode light-matter interactions and achieve some potential applications for multimode sensors.

OCIS codes: (240.5420) Polaritons; (160.4890) Organic materials; (160.5298) Photonic crystals; (260.0260) Physical optics.

https://doi.org/10.1364/OL.41.005740

In recent years, photon-exciton interactions have attracted continuous interest, especially the strong coupling, where the energy exchange between photons and excitons prevails over their damping rates. Strong coupling results in the formation of quasi-particles named polaritons, with both light-like and matter-like features, which are good candidates to explore some fundamental problems, such as Bose–Einstein condensation [1–3]. Moreover, polariton nanolasers [4–6] and transistors [7] offer possibilities to realize all-optical circuits at the nanoscale. Owing to the higher binding energy, saturation density, and oscillator strength, Frenkel excitons in organic semiconductors become a feasible substitution for the Wannier excitons in inorganic semiconductors. Organic semiconductors used most often include porphyrines [8], J-aggregates [9–18], and organic crystals [19]. Strong couplings between photons and Frenkel excitons have been realized in many photonic systems, such as multilayered distributed Bragg reflectors (DBRs) [8–10,19], optical microcavities [11,12], and plasmonic nanostructures [13–18], offering various platforms to guide and manipulate polaritons at the nanoscale.

Although most work on strong coupling explores interactions between a single excitonic mode and a single photonic mode, some attention has been paid to multimode hybrid coupling in which the excitonic mode couples to more than one photonic modes. One approach to realize the multimode coupling is to employ coupled cavities [20,21] or a planar cavity with an extended optical path length [22], which contains multiple cavity modes. Another approach is to design nanostructures supporting different plasmonic modes [23] or sustaining both cavity and plasmonic modes [24]. However, most of these systems are complicated and need further fabrication or evaporation after depositing organic semiconductors, which may more or less affect the quality of excitons. Here, we design an open system employing the photonic quasicrystal to provide multiple photonic modes, where no further fabrication is needed after spinning the J-aggregates onto it, without any damage to the organic semiconductor. In this way, such an open system can be used to offer multimode hybrid interactions, which may inspire related studies on multimode light-matter interactions and achieve some potential applications, such as multimode sensors and spectroscopy.

Photonic quasicrystals built by dielectric multilayers have been widely studied [25–29], and excitonic polaritons in such quasicrystals combined with inorganic quantum wells have also been realized [30–32]. One-dimensional photonic quasicrystals can be generated utilizing a substitution rule based on two building blocks, exhibiting long-range order, lacking translational symmetry, but with properties of self-similarity. Employing the Fibonacci series, using the two building blocks A and B with a refractive index of n_A and n_B, we can construct a photonic quasicrystal whose central resonant wavelength is λ. In this way, the Fibonacci sequence starts with the two segments, A with a thickness $t_A = \lambda/4n_A$ and B with a thickness $t_B = \lambda/4n_B$, and operates with the iterative rules A → B and B → BA to build successive chains. According to this rule, the eighth member of the Fibonacci series, labeled as S_8, should be in the sequence of BABBABABBABBABABBABAB, as schematically described in Fig. 1(a). Following the sequence of S_8, we utilize two dielectric materials to build the sample in this Letter, i.e., Ta_2O_5 as the segment "A," with $n_A = 2.1$, and

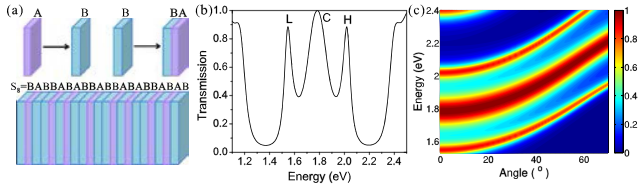

Fig. 1. (a) Schematic description of the photonic quasicrystal in a Fibonacci sequence, which starts with two segments, i.e., A and B, and operates with the iterative rules A → B and B → BA to build successive strings. (b) Calculated reflection spectrum under normal incidence and (c) the dispersion map of the photonic quasicrystal.

SiO_2 as the segment "B," with $n_B = 1.46$. In order to realize the central resonant wavelength at 697 nm (corresponding to 1.78 eV), the thickness of the building blocks is designed to be $t_A = 83$ nm and $t_B = 119$ nm, respectively. The transmission spectrum of this photonic quasicrystal can be calculated by the transfer matrix method [25,26], and the result is shown in Fig. 1(b). There are three photonic modes, where the central mode around 1.78 eV is marked as C, the lower-energy one around 1.55 eV is marked as L, and the higher-energy one around 2.02 eV is marked as H. In order to see the dispersion of these photonic modes, we calculate the transmission spectra by sweeping incident angles, and display the results in Fig. 1(c). The energies of all three modes increase with the incident angles, creating the possibility to successively interact with the same excitonic mode. Consequently, such a photonic quasicrystal can be used to realize multimode photon-exciton coupling when combined with semiconductors.

To experimentally demonstrate this phenomenon, we use the electron beam evaporation method to deposit the dielectric multilayers, and choose TDBC (5,6-Dichloro-2-[[5,6-dichloro-1-ethyl-3-(4-sulfobutyl)-benzimidazol-2-ylidene]-propenyl]-1-ethyl-3-(4-sulfobutyl)-benzimidazolium hydroxide, inner salt, sodium salt) to form J-aggregates acting as organic semiconductor. Following the simulation parameters, we deposit SiO_2/Ta_2O_5 multilayers onto K9 glass substrate, and then directly spin J-aggregates onto the top surface, as schematically described in Fig. 2(a). The optical photos of the photonic quasicrystal sample and the sample covered by J-aggregates are, respectively, displayed in Fig. 2(b). From the SEM photo of the photonic quasicrystal intersecting surface, we can clearly see the Fibonacci sequence composed of the dielectric multilayers. The experimentally measured transmission spectrum of this photonic quasicrystal is shown in Fig. 2(c), and there are three transmission peaks corresponding to the modes labeled as "L," "C," and "H" in Fig. 1(b), matching well with the calculation results. Then we measure the absorption and the photoluminescence (PL) spectra of the J-aggregates spun on glass substrate, as shown in Fig. 2(d), indicating the exciton energy to be around 2.11 eV, which is close to the energies of the photonic modes, offering the possibility of the strong coupling between the excitons and the photonic modes.

Gradually increasing the incident angles to measure the transmission spectra, we can get the dispersion of the optical modes. We first measure the sample without J-aggregates, and the dispersion map is drawn in Fig. 3(a). Besides the experimental results, we also fit the photonic modes by the white dashed lines and indicate the exciton energy by the black dashed line. As the incident angle increasing, the energies of

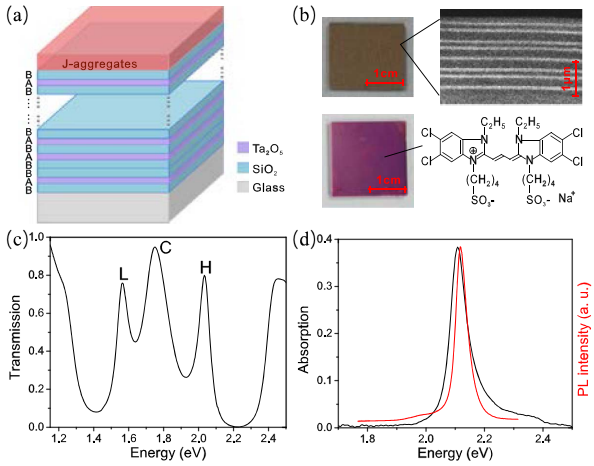

Fig. 2. (a) Schematic description of the sample, a photonic quasicrystal covered by the organic semiconductor. (b) Top left one is the optical photo of the photonic quasicrystal sample, and the top right one is the SEM photo of its intersecting surface. The bottom left one is the optical photo of the quasicrystal sample covered by the spin-coated J-aggregates, and the right displays the chemical formula of TDBC used to form J-aggregates. (c) Experimentally measured transmission spectra of the photonic quasicrystal sample under normal incidence. (d) Measured absorption spectrum (black line) and the normalized PL spectrum (red line) of the J-aggregates.

modes H and C successively go across the energy of the excitons while the energy of mode L approaches it, indicating the possibility of strong coupling. To achieve this, we cover this sample with J-aggregates and then measure its transmission spectra under different incident angles. Figure 3(b) shows some transmission spectra under different incident angles, in which we trace the peaks by the dashed lines to show the tendency more clearly. There are five modes dispersing with the incident angles. We can find obvious anti-crossing between the two red (or blue) dashed lines, which is the so-called Rabi splitting because of strong coupling. Therefore, these modes are hybridized upper polariton bands (UPBs) and lower polariton bands (LPBs). The two traced by the red dashed lines (marked as H-LPB and H-UPB) come from the coupling between mode H and excitons; those traced by the blue dashed lines (C-LPB and C-UPB) come from the coupling between mode C and excitons; and the one traced by the olive dashed line (L-LPB) comes from the coupling between mode L and excitons. In this way, there should be another polariton band L-UPB, which may be observable at larger incident angles. Unfortunately, it cannot be clearly observed due to the limit of our measurement.

To show the hybrid polariton bands more distinctly, we draw the transmission spectra into the two-dimensional dispersion map in Fig. 3(c). It shows that the modes H, C, and L successively couples with the excitons at different incident angles, leading to the Rabi splitting and generating hybrid polariton bands. The five observable polariton bands, H-UPB, H-LPB, C-UPB, C-LPB, and L-LPB, correspond to those marked in Fig. 3(b). To further analyze these polariton bands, we employ the model of coupled harmonic oscillators to fit the experimental results. As the photonic modes H, L, and C, respectively, couple with the excitons, the resulting polariton bands consist of a photonic state $|ph_i\rangle$ ($i = H$, C, or L) and

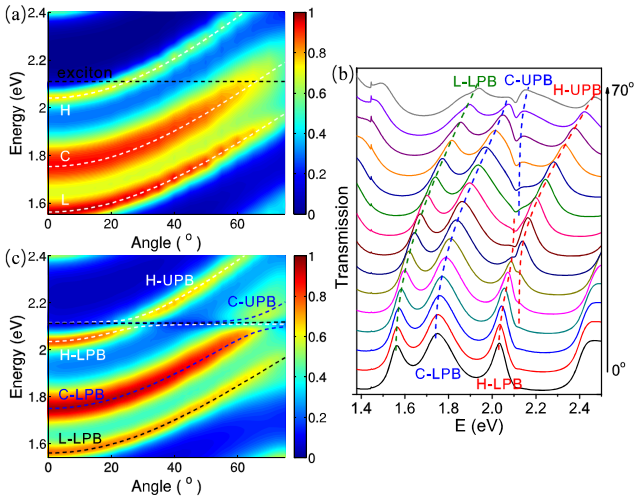

Fig. 3. (a) Experimentally measured dispersion map of the photonic quasicrystal sample. The white dashed lines fit the three photonic modes and the black dashed line indicates the energy of the excitons in J-aggregates. (b) Transmission spectra of the sample covered by J-aggregates under different incident angles, and the dashed lines trace the polariton bands. (c) Two-dimensional dispersion map of the sample covered by the J-aggregates. The dashed lines are the calculated results fitting the polariton bands.

an excitonic state $|e\rangle$. Using these states as a basic set, we get the non-Hermitian Hamiltonian as

$$\mathcal{H} = \begin{pmatrix} E_{\text{phi}}(\theta) & \hbar\Omega_i/2 \\ \hbar\Omega_i^*/2 & E_{\text{ex}} \end{pmatrix} - i\hbar \begin{pmatrix} \gamma_{\text{phi}} & 0 \\ 0 & \gamma_{\text{ex}} \end{pmatrix}, \quad (1)$$

where $E_{\text{phi}}(\theta)$ (i = H, C, or L) represents the energy of the photonic mode H, C, or L, E_{ex} is the energy of the excitons, $\hbar\Omega_i$ is the coupling energy between the photonic mode and the excitons, and γ_{phi} and γ_{ex} are the damping frequency of the photonic mode and the excitons, respectively. Here, we simplify the model by excluding the cross-damping terms, which describe the incoherent exchange of energy between the photonic modes and excitons [14,33]. For every photonic mode, this model predicts the formation of two polariton states because of the strong coupling, i.e., the LPB and the UPB in experiment. Every polariton state can be written as $|P_i^{L(U)}\rangle = \alpha_i^{L(U)}|ph_i\rangle + \alpha_e^{L(U)}|e\rangle$, whose eigenenergy can be calculated by diagonalizing the Hamiltonian, where $|\alpha_i^{L(U)}|^2$ and $|\alpha_e^{L(U)}|^2$ correspond to the relative mixing fractions of the photonic mode and the excitons in LPB (or UPB). To make a best fit to the experimental data, we find the value of the coupling energy to be $\hbar\Omega_H = 67$ meV, $\hbar\Omega_C = 93$ meV, and $\hbar\Omega_L = 85$ meV. The calculated eigenenergies of the six polariton bands in this system are described by the dashed lines in Fig. 3(c), and all these results fit well with the experimental data.

Based on the experimental data and the fitting results, we can also retrieve the relative mixing fractions $|\alpha_i^{L(U)}|^2$ and $|\alpha_e^{L(U)}|^2$ in the polariton bands, which are shown in Fig. 4. For the lower polariton bands H-LPB, C-LPB, and L-LPB, they are mainly composed of the photonic modes at small incident angles. As the incident angle increases, these polariton bands successively approach the excitonic mode, accompanied

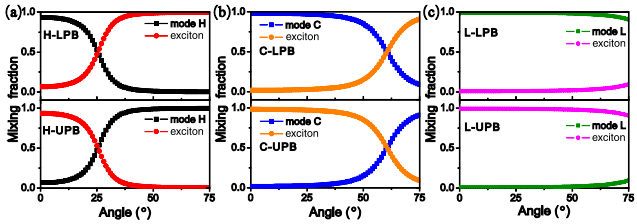

Fig. 4. Mixing fractions of the photonic modes and the excitons in the polariton bands, retrieved from the experimental data.

by the increase of the exciton mixing fractions and the decrease of the photonic mode mixing fractions. For the upper polariton bands H-UPB, C-UPB, and L-UPB, the excitonic component is the chief ingredient at small incident angles. The UPBs gradually leave the excitonic mode as the angle increases; as a result, the photonic component predominates at larger angles. In this way, although these six polariton bands come from couplings between excitons and different photonic modes, the mixing fractions in all the LPBs (or all the UPBs) behave in the similar way.

Moreover, we can also fit the spectra line width of the measured polariton band by employing the Hamiltonian in Eq. (1), which is related to the imaginary part of the eigenenergy. As shown in Fig. 5, the circles and triangles describe the full width at half-maximum (FWHM) of the polariton bands in the experimental spectra shown in Fig. 3(c), while the asterisks represent the ones calculated using the FWHM of the excitonic mode shown in Fig. 2(d) and those of the photonic modes in Fig. 3(a). For all the observable polariton bands in our experiment, the calculated results of the FWHM fit well with the measured ones. It means that, besides the energy dispersion features, the polariton band also inherits the damping behaviors from both the photonic mode and the excitons. In this case, the damping properties of the polariton band can be tuned by designing the mixing fractions of the photonic mode and the excitons, which may be employed to meet some requirements in potential applications.

In summary, we have proposed and experimentally demonstrated multiple strong couplings in an organic-dye-attached photonic quasicrystal, where all the fabrication processes are done before spin-coating the organic semiconductor, applying no affection to the exciton quality. In this system, three photonic modes are simultaneously introduced to interact with the excitons. As a result, three strong couplings successively occur at different incident angles, resulting in six polariton bands. By retrieving from the experimental data, we also get the mixing fractions of the photonic modes and the excitons in these

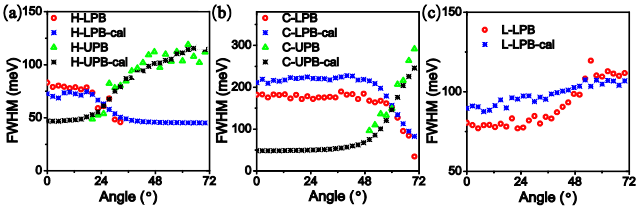

Fig. 5. FWHM of the five observable polariton bands, where the circles and the triangles represent the FWHM from the experimentally measured polariton spectra, and the asterisks depict the calculated FWHM.

hybrid bands, finding out that the components in the same kind of polariton bands (all LPBs or all UPBs) vary with the incident angles in the similar way. Employing the model of coupled harmonic oscillators, both the energy and the line width of the polariton spectra are well fitted. Therefore, the polariton bands inherit light-like features from the photonic modes and matter-like features from the excitons, modifying both the energy dispersion and the line width of the spectra.

Such an open system can be optimized by tuning the substitution rule of the photonic quasicrystal, to match different requirements of both the number and the quality factors of the photonic modes. In this way, it can be employed to offer multimode photon-exciton strong couplings, which may inspire related studies about hybrid light-matter interactions and achieve some potential applications, such as multimode sensors and optical spectroscopy.

Funding. National Natural Science Foundation of China (NSFC) (11634005, 61475070, 11474157, 11674155, 11321063, 91321312).

REFERENCES

1. J. Kasprzak, M. Richard, S. Kundermann, A. Baas, P. Jeambrun, J. M. J. Keeling, F. M. Marchetti, M. H. Szymanska, R. André, J. L. Staehli, V. Savona, P. B. Littlewood, B. Deveaud, and L. S. Dang, Nature **443**, 409 (2006).
2. J. D. Plumhof, T. Stöferle, L. Mai, U. Scherf, and R. F. Mahrt, Nat. Mater. **13**, 247 (2014).
3. K. S. Daskalakis, S. A. Maier, R. Murray, and S. Kéna-Cohen, Nat. Mater. **13**, 271 (2014).
4. L. S. Dang, D. Heger, R. André, F. Bœuf, and R. Romestain, Phys. Rev. Lett. **81**, 3920 (1998).
5. P. Senellart and J. Bloch, Phys. Rev. Lett. **82**, 1233 (1999).
6. S. Christopoulos, G. B. H. Högersthal, A. J. D. Grundy, P. G. Lagoudakis, A. V. Kavokin, and J. J. Baumberg, Phys. Rev. Lett. **98**, 126405 (2007).
7. D. Ballarini, M. D. Giorgi, E. Cancellieri, R. Houdré, E. Giacobino, R. Cingolani, A. Bramati, G. Gigli, and D. Sanvitto, Nat. Commun. **4**, 1778 (2013).
8. D. G. Lidzey, D. D. C. Bradley, M. S. Skolnick, T. Virgili, S. Walker, and D. M. Whittaker, Nature **395**, 53 (1998).
9. D. G. Lidzey, D. D. C. Bradley, T. Virgili, A. Armitage, and M. S. Skolnick, Phys. Rev. Lett. **82**, 3316 (1999).
10. S. Pirotta, M. Patrini, M. Liscidini, M. Galli, G. Dacarro, G. Canazza, G. Guizzetti, D. Comoretto, and D. Bajoni, Appl. Phys. Lett. **104**, 051111 (2014).
11. D. Ballarini, M. D. Giorgi, S. Gambino, G. Lerario, M. Mazzeo, A. Genco, G. Accorsi, C. Giansante, S. Colella, S. D'Agostino, P. Cazzato, D. Sanvitto, and G. Gigli, Adv. Opt. Mater. **2**, 1076 (2014).
12. S. Hayashi, Y. Ishigaki, and M. Fujii, Phys. Rev. B **86**, 045408 (2012).
13. J. Bellessa, C. Bonnand, J. C. Plenet, and J. Mugnier, Phys. Rev. Lett. **93**, 036404 (2004).
14. W. Wang, P. Vasa, R. Pomraenke, R. Vogelgesang, A. D. Sio, E. Sommer, M. Maiuri, C. Manzoni, G. Cerullo, and C. Lienau, ACS Nano **8**, 1056 (2014).
15. E. Eizner and T. Ellenbogen, Appl. Phys. Lett. **104**, 223301 (2014).
16. E. Karademir, S. Balci, C. Kocabas, and A. Aydinli, Opt. Express **22**, 21912 (2014).
17. B. G. DeLacy, O. D. Miller, C. W. Hsu, Z. Zander, S. Lacey, R. Yagloski, A. W. Fountain, E. Valdes, E. Anquillare, M. Soljačić, S. G. Johnson, and J. D. Joannopoulos, Nano Lett. **15**, 2588 (2015).
18. G. Zengin, M. Wersäll, S. Nilsson, T. J. Antosiewicz, M. Käll, and T. Shegai, Phys. Rev. Lett. **114**, 157401 (2015).
19. R. J. Holmes and S. R. Forrest, Phys. Rev. Lett. **93**, 186404 (2004).
20. S. Stelitano, G. D. Luca, S. Savasta, L. M. Scolaro, and S. Patané, Appl. Phys. Lett. **95**, 093303 (2009).
21. A. Ridolfo, S. Stelitano, S. Patanè, S. Savasta, and R. Girlanda, Phys. Rev. B **81**, 075313 (2010).
22. D. M. Coles and D. G. Lidzey, Appl. Phys. Lett. **104**, 191108 (2014).
23. S. Balci and C. Kocabas, Opt. Lett. **40**, 3424 (2015).
24. K. Zhang, W. B. Shi, D. Wang, Y. Xu, R. W. Peng, R. H. Fan, Q. J. Wang, and M. Wang, Appl. Phys. Lett. **108**, 193111 (2016).
25. M. Kohmoto, B. Sutherland, and K. Iguchi, Phys. Rev. Lett. **58**, 2436 (1987).
26. W. Gellermann, M. Kohmoto, B. Sutherland, and P. C. Taylor, Phys. Rev. Lett. **72**, 633 (1994).
27. T. Hattori, N. Tsurumachi, S. Kawato, and H. Nakatsuka, Phys. Rev. B **50**, 4220 (1994).
28. Z. V. Vardeny, A. Nahata, and A. Agrawal, Nat. Photonics **7**, 177 (2013).
29. R. W. Peng, Y. M. Liu, X. Q. Huang, F. Qiu, M. Wang, A. Hu, S. S. Jiang, D. Feng, L. Z. Ouyang, and J. Zou, Phys. Rev. B **69**, 165109 (2004).
30. J. Hendrickson, B. C. Richards, J. Sweet, G. Khitrova, A. N. Poddubny, E. L. Ivchenko, M. Wegener, and H. M. Gibbs, Opt. Express **16**, 15382 (2008).
31. M. Werchner, M. Schafer, M. Kira, S. W. Koch, J. Sweet, J. D. Olitzky, J. Hendrickson, B. C. Richards, G. Khitrova, H. M. Gibbs, A. N. Poddubny, E. L. Ivchenko, M. Voronov, and M. Wegener, Opt. Express **17**, 6813 (2009).
32. D. Tanese, E. Gurevich, F. Baboux, T. Jacqmin, A. Lemaître, E. Galopin, I. Sagnes, A. Amo, J. Bloch, and E. Akkermans, Phys. Rev. Lett. **112**, 146404 (2014).
33. P. Zeng, J. Cadusch, D. Chakraborty, T. A. Smith, A. Roberts, J. E. Sader, T. J. Davis, and D. E. Gómez, Nano Lett. **16**, 2651 (2016).